Int J Thermophys (2007) 28:1490–1508
DOI 10.1007/s10765-007-0294-8

# A Study of the Flow through Capillary Tubes Tuned for a Cooling Circuit with Saturated Fluorocarbon Refrigerants

**Vaclav Vacek · Vaclav Vinš**

Published online: 16 October 2007


**Abstract** Capillary tube expansion devices are widely used in refrigeration equipment; nevertheless, the mechanism of the flow is still not fully described and understood, so the experimental verification of most predictions is still necessary. A modified numerical model of capillary flow has been developed both for standard refrigerants and with emphasis for saturated fluorocarbon ($C_2F_{2n+2}$) refrigerants. These refrigerants have several unique properties (high dielectric performance, chemical stability, and radiation resistance). Therefore, they can be used in some special applications, where other common fluids cannot be applied. The main aim of this study was to prepare a practical capillary flow model, which would improve the procedure of predicting the behavior of capillary tubes for cooling circuits of particle detectors being built at the international CERN laboratory in Geneva. The generated numerical model was verified through available data from the literature and also via measurements performed in a real cooling circuit with pure, oil-free octafluoropropane ($C_3F_8$) refrigerant.

**Keywords** Capillary tube · Cooling circuit · Fluorocarbon refrigerant · Model comparisons · Two-phase flow

Paper presented at the Seventeenth European Conference on Thermophysical Properties, September 5–8, 2005, Bratislava, Slovak Republic.

V. Vacek (✉) · V. Vinš
Department of Applied Physics, Faculty of Mechanical Engineering, Czech Technical University in Prague, Technicka 4, Prague 6, 16607 Czech Republic
e-mail: vaclav.vacek@cern.ch

**Nomenclature**

| | |
|---|---|
| $c_p$ | Specific heat ($J \cdot kg^{-1} \cdot K^{-1}$) |
| $e$ | Specific energy ($e = h + v^2/2 = E + p/\rho$) ($J \cdot kg^{-1}$) |
| $f$ | Friction factor |
| $h$ | Enthalpy ($J \cdot kg^{-1}$) |
| $\dot{m}$ | Mass flow rate ($kg \cdot s^{-1}$) |
| $p$ | Pressure (Pa) |
| $q$ | Heat flux ($W \cdot m^{-2}$) |
| $s$ | Entropy ($J \cdot kg^{-1} \cdot K^{-1}$) |
| $t$ | Time (s) |
| $v$ | Velocity ($m \cdot s^{-1}$) |
| $z$ | Axial coordinate (m) |
| $A$ | Capillary inner cross section ($m^2$) |
| $E$ | Energy (sum of internal energy and kinetic energy) ($J \cdot kg^{-1}$) |
| $ID$ | Inner diameter (m) |
| $K_z$ | Body forces (gravity) ($m \cdot s^{-2}$) |
| $L$ | Capillary tube length (m) |
| $P$ | Capillary inner perimeter (m) |
| $Re$ | Reynolds number |
| $S$ | Slip ratio |
| $T$ | Temperature (K) |
| *Greek Letters* | |
| $\alpha$ | Void fraction |
| $\delta$ | Capillary wall roughness (m) |
| $\rho$ | Density ($kg \cdot m^{-3}$) |
| $\tau$ | Shear stress (Pa) |
| $x$ | Vapor quality |
| $\Delta z$ | Control volume length (m) |
| $\Phi_{LO}$ | Two-phase multiplier |
| *Subscripts* | |
| amb | Ambient |
| crit | Critical flow conditions |
| dis | Discharge—conditions at capillary outlet |
| evap | Evaporation |
| $i$ | Control volume inlet (point $i$ of the computational grid) |
| $i+1$ | Control volume outlet (point $i+1$ of the computational grid) |
| in | Capillary inlet |
| sat | Saturation properties |
| TP | Two-phase |
| w | Condition at the capillary inner wall |
| *Superscripts* | |
| g | Vapor phase |
| l | Liquid phase |
| – | Arithmetical average over a control volume |
| $\sim$ | Integral average over a control volume |

## 1 Introduction

Capillary tubes are mostly copper, copper–nickel, or aluminum tubes with a small inner diameter, often between 0.5 and 1.5 mm, with a length varying between 0.4 and 6 m. They are widely used as the expansion devices in smaller refrigeration and air conditioning systems, since they are relatively simple and inexpensive parts. Capillaries substitute for more expensive and complex thermostatic valves. Nevertheless, one can find other reasons for their use in highly specialized cooling circuits. For instance, capillary tubes are used in some complex cooling systems for particle detectors installed at the Large Hadron Collider (LHC) of the CERN particle physics laboratory in Geneva. In such an application, one has to face many additional problems such as space constraints, and surrounding environment with high magnetic fields or radiation levels. Other problems arise from the manifolding of a large number of individual evaporators and from the placement of their capillaries in an inaccessible zone, bounded between the 30 m distant pressure regulator (the flow control element) and the backpressure regulator (evaporation pressure control), with the compressor–condenser unit located even farther (∼150 m) away. All these additional demands preclude the use of more sophisticated throttling devices than the capillary tubes.

Saturated fluorocarbon refrigerants with the chemical structure ($C_nF_{2n+2}$), which previously had an application in radar and supercomputer immersion cooling and also as heat transfer media in vapor phase soldering, are used in the cooling circuits at CERN. They have valuable properties (high dielectric performance, chemical stability, and radiation resistance) which make them favorable for such special applications compared to the standard classes of refrigerants used in the cooling industry.

The main aim of our study was to prepare a modified numerical simulation of the fluorocarbon refrigerant flow through the capillary tube, which could be used for an effective prediction of the capillaries designed for the cooling circuits of 'ATLAS,' 'ALICE,' and 'TOTEM' experiments built for the CERN LHC. Many preparatory experimental measurements on both single-phase flow and on evaporative cooling circuits had to be performed to test the simulation predictions. The model was successfully used for the trimming of a large quantity of capillary tubes having different geometrical parameters and various operating conditions.

## 2 Some Previous Studies and Literature Review

The typical pressure distribution over the capillary tube is shown in Fig. 1a. The first small pressure drop (point 0–point 1) occurs at the inlet, as the subcooled liquid coolant enters the capillary. The pressure linearly decreases until the saturation pressure is reached at point 2. The outlet conditions are defined by point 3, where the flow can reach a speed anywhere up to the critical speed (the local speed of sound). An uncontrolled expansion connected with shock-wave generation might occur between points 3 and 4 for the case of critical conditions at the capillary outlet.

Figure 1b illustrates the pressure drop according to the complex capillary flow models described, for instance, by Mikol [1] or Li et al. [2]. They reported that the evaporating flow through a capillary consists of four different regions. There are not

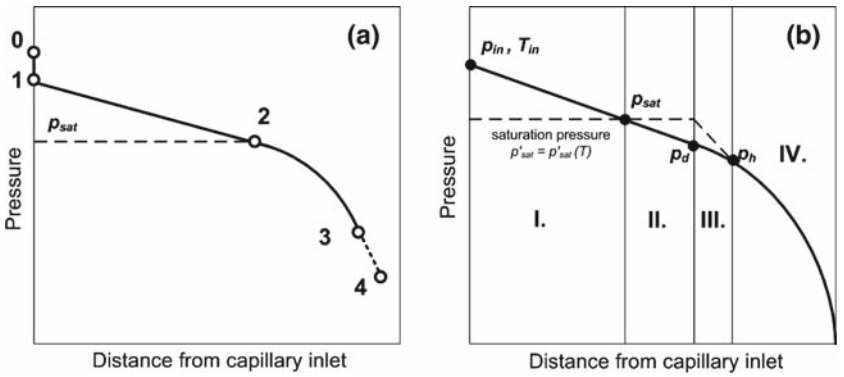


**Fig. 1** (**a**) Pressure distribution along the capillary tube and (**b**) regions of capillary flow: I—subcooled single liquid phase, II—metastable single liquid phase, III—metastable two-phase region (liquid–vapor), and IV—thermodynamic equilibrium two-phase region (liquid–vapor)

only two thermodynamic equilibrium phenomena of the subcooled liquid and two-phase mixture, but also two metastable regions. The saturation condition and the flash point define the metastable single liquid region-II. The evaluation of the pressure of vaporization at the flash point has been studied by Chen et al. [3] and Lackme [4]. Region III is a zone, where both the liquid and two-phase flow remains in a metastable state. Koizumi and Yokoyama [5] also investigated the metastable regions and measured the temperature and pressure development along glass capillaries, proving the existence of metastable regions both from their measurements and from visual observations.

Problems related to global warming and ozone depletion effects have required the introduction of new alternative refrigerants by the cooling industry. This also drives demands for more accurate and general methods for predicting the thermal- and fluid-dynamic behavior of capillaries. A number of theoretical and experimental studies have been carried out, especially over the past decade.

The majority of theoretical research assumes just two thermodynamic equilibrium regions of capillary flow and uses homogeneous two-phase flow with the same velocities for both vapor and liquid. For instance, Bansal and Rupasinghe [6] and Kritsadathikarn et al. [7] have presented models of homogeneous two-phase flow through an adiabatic capillary tube. Sami and Tribes [8] presented a numerical study of capillary tube performance, operating with alternative refrigerants and their binary mixtures.

Wong and Ooi [9] developed a numerical model with separated two-phase flow, solved with the slip ratio correlation of Miropolskiy et al. [10] and the approximation of a two-phase frictional pressure gradient of Lin et al. [11]. Comparisons with experimental data and simplified homogeneous models showed that the separate numerical model gave a better prediction of the capillary tube performance. Wongwises and Chan [12] studied the effects of various correlations of the slip ratio, frictional pressure gradient, and friction factor on the predictions computed with a separated model of adiabatic capillary flow. Bansal and Wang [13] presented another numerical model of the adiabatic capillary flow including a liquid metastable region. They generated a

'full range simulation diagram', which helped explain the choked flow phenomenon graphically.

All the above-mentioned studies assume pure adiabatic capillary flow. Sinpiboon and Wongwises [14] developed a numerical study of refrigerant flow through a non-adiabatic capillary. The mathematical model is categorized into three different cases, depending on the position of the capillary in the heat exchanger. Another model providing a non-adiabatic capillary flow solution was introduced in a numerical study by Escanes and Pérez-Segarra [15]. The set of four differential equations is solved on the basis of a one-dimensional finite volume method. The heat transfer coefficient is defined from Gnielinski correlations [16] and assumes the known temperature distribution on the capillary inner wall.

An advanced complex model of capillary flow was recently presented by García-Valladares and Pérez-Segarra [17]. Their model represents a solution of capillary flow with all four partial regions in an adiabatic and non-adiabatic capillary tube. Other authors who generated a numerical model of non-adiabatic capillary flow are Xu and Bansal [18]. They introduced simulation of the flow through a capillary-suction line heat exchanger common in smaller vapor cooling systems.

The numerical models are somewhat time-consuming and they require advanced programming skills, so this approach to the problem is not always easy for engineers. So, analytical approximation models are also favored in everyday practice, even if they are less precise and do not describe the capillary behavior in detail. Novel approximate analytical approaches were developed, for instance, by Yilmaz and Ünal [19] and by Zhang and Ding [20].

Let us conclude with the experimental study of the capillary flow presented by Melo et al. [21]. The two-phase flow of three different refrigerants—R12, R134a, and HC-600a—was investigated for eight capillaries with varied combinations of length, diameter, and tube roughness. A conventional, dimensionless analysis was utilized to derive correlations to predict the mass flow rates through capillary tubes.

## 3 Objectives, Methodology, and Preparation Studies

The main objective of our study was to develop a numerical model of the capillary flow that would improve and shorten the procedure of prediction of the behavior of capillary tubes designed for cooling circuits of experiments being built at CERN laboratory. All these systems work with saturated fluorocarbon refrigerants, whose flow behavior within the capillary tube had not been investigated before. Behavior in a number of different capillary configurations, having inner diameters from 0.45 to 1.2 mm and lengths between 0.4 and 6.0 m, had to be predicted.

Proper predictions of the capillary-tube performance required several preparation activities due to the usage of uncommon refrigerants and large number of capillary tubes having different dimensions. Thermodynamic and transport properties of the refrigerant used in the model, and also some information about capillary parameters had to studied. The correct evaluation of the inner diameter (ID) and inner surface roughness are particularly important.

Thermophysical data for our target refrigerants, i.e., R218, octafluoropropane (referred to as $C_3F_8$ in the text) and R610, i.e., perfluorobutane (referred to as $C_4F_{10}$ in the text), are not very copious in the open literature when compared to the standard group of refrigerants. We have used the REFPROP database [22] with provisional data files to generate the required properties and correlated them with our previously published measurements realized with saturated fluorocarbons and their mixtures [23,24]. The retrieved data were than mostly fitted via polynomial or exponential functions in the regions relevant to our studies.

The inside diameters of our capillaries (made of stainless steel, copper, copper–nickel, and aluminum) were measured usually by two methods. In the first weighing method—the capillary tubes were filled with saturated fluorocarbon liquids (perfluorohexane—$C_6F_{14}$ or perfluorooctane—$C_8F_{18}$) having densities 1.7 times that of water at normal laboratory temperatures. A precise balance determined the mass of the liquid in the capillary and allowed calculation of the average inner diameter. The second method, applied to a number of capillary sample cuts from the same batch, was an optical inspection. Both methods provided similar values of the inner diameter with an uncertainty of about $\pm 0.008$ mm; however, in case of optical inspection, the cut of the capillary tube must be made rather carefully to assure that the capillary cross section is not sqeezed. The weighing method was found more practical as the capillary tube was not damaged during the measurement and as the average value of inner diameter was found. Precise knowledge of this value is crucial for successful prediction of capillary tube performance. Moreover, the weighing method brings other advantages. As all fluorinert liquids behave as solvents, each capillary tube was cleaned during its installation into the cooling circuit and the residual water was driven out.

In order to verify or estimate the inner surface capillary roughness and consequently to use the most suitable relation for the friction factor led us to a detailed investigation of the liquid-phase flow through the capillaries. The influence of the inner surface capillary roughness can be seen in Fig. 2.

For liquid-phase flow studies, at laboratory temperatures, we used the setup shown in Fig. 3. The $C_6F_{14}$ and $C_8F_{18}$ saturated fluorocarbon liquids were utilized since they exhibit similar properties (density, viscosity, surface tension, etc.) at laboratory temperatures to those of $C_3F_8$ and $C_4F_{10}$ to be used in the real cooling circuit at the expected operating temperatures.

Prior to the capillary studies, we have measured some relevant thermophysical properties of $C_6F_{14}$ and $C_8F_{18}$ using an Anton Paar DSA 48 analyzer. The density and speed of sound were determined in the appropriate temperature region. The density of liquid $C_6F_{14}$ can be expressed as $\rho(T) = 1755.5 - 2.936\,T$ between 5 and 40°C, while that of the higher boiling point $C_8F_{18}$ can be approximated by $\rho(T) = 1825.5 - 2.6036\,T$ between 5 and 65°C.

Characteristics of various different capillaries were evaluated via the measured pressure drop using a precise differential pressure sensor together with a reference absolute pressure transducer. The mass flow was monitored with a precision coriolis-type mass flow meter having an uncertainty of $\pm 0.03\,\mathrm{g \cdot s^{-1}}$, and was also initially checked through the direct weighing method. Some 18 capillary samples were investigated (ranging in ID from 0.6 to 1.1 mm and in length from 0.7 to 3 m). The four different friction factor approximations (Churchill [6], Colebrook [7], Haaland [25],

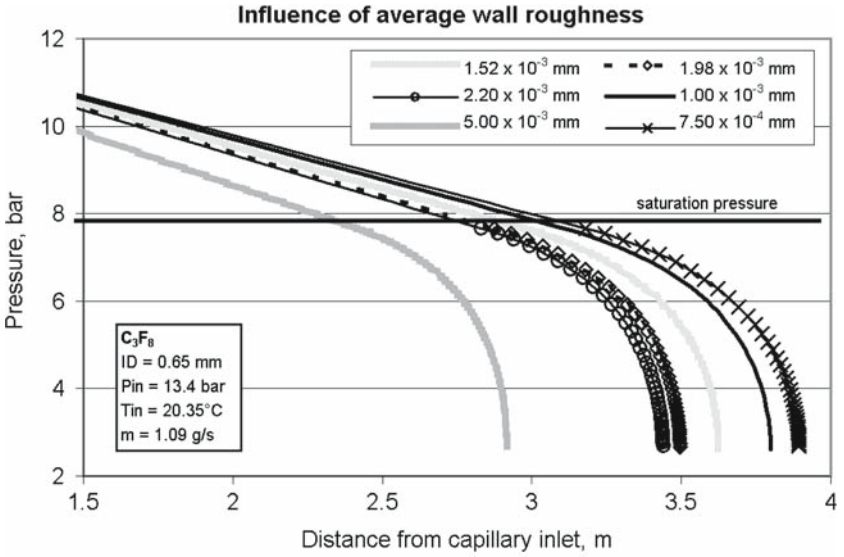


**Fig. 2** Inner wall surface roughness impact on the capillary length and pressure profile

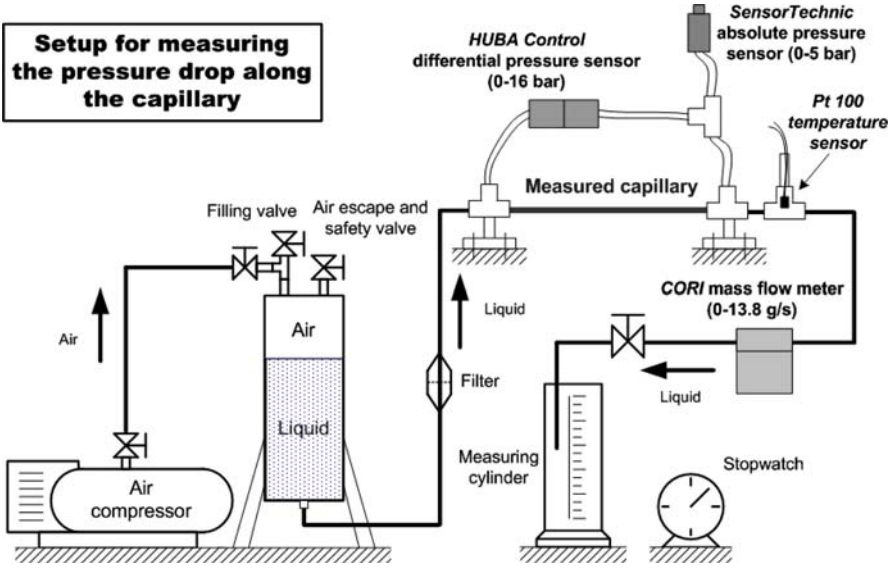


**Fig. 3** Experimental setup for capillary behavior in liquid phase flow ($C_6F_{14}$, $C_8F_{18}$)

and the classical equation) usually used in capillary flow models were compared with our measured results. Our evaluations resulted in a conclusion to use the Colebrook friction relation for our studies with a copper capillary, with an inner surface roughness selected to be around $2 \times 10^{-6}$ m. Differences between the correlations and experimental data are shown in Fig. 4.

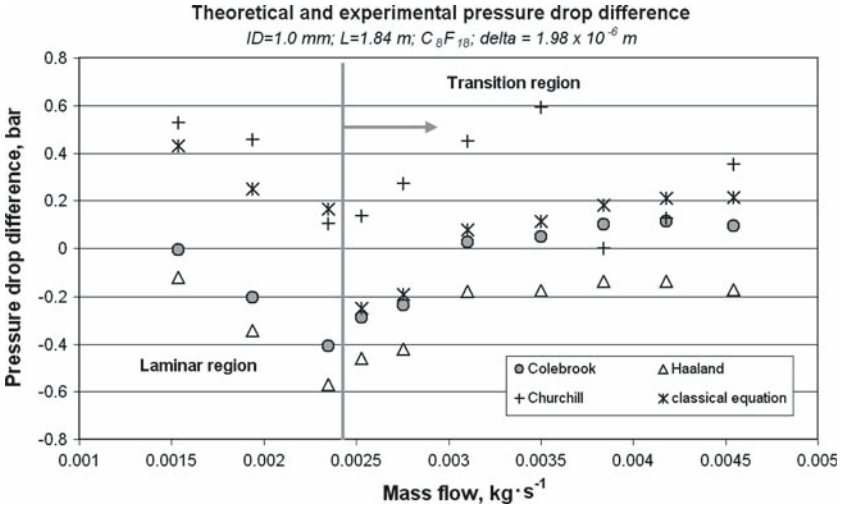


**Fig. 4** Evaluation of the different friction factors against the measured data

## 4 Numerical Model of Capillary Flow

The aim of this study was to develop a steady-state numerical simulation of capillary flow behavior under either adiabatic or non-adiabatic conditions. The current study was partly inspired by some models presented in the literature (mainly [12], [15], and [17]). The model assumes two equilibrium regions of the capillary flow and provides solutions for both the homogeneous and the separated two-phase flow. The results obtained give the information about the development of all the main flow characteristics (pressure, temperature, vapor quality, etc.) along the capillary tube.

The model allows the solving of the two main capillary flow cases. In the first mode, the capillary tube length is solved from known input parameters including the given refrigerant-mass flow rate. In the second mode, the mass flow rate for the capillary tube of given length is found on the basis of the capillary tube length solution and the optimization approach based upon an 'interval-halving' method. As the model should serve for the design of capillary tubes to be used in specific cooling circuits of particle detectors, the simulation was modified to solve capillary flows of $C_3F_8$ (for ATLAS and TOTEM experiments) and $C_4F_{10}$ (for ALICE experiment). Besides these fluids, the capillary flow of standard refrigerants such as R12 or R134a can be modeled as well. The effect of different semi-empirical correlations for the refrigerant capillary flow (friction factor, two-phase viscosity, etc.) on the accuracy of the simulated data was also investigated.

### 4.1 Mathematical Formulation and Numerical Solution

The governing equations of the flow (continuity, momentum, energy, and entropy) in a differential form were discretized using a one-dimensional finite volume method.

This approach brings several advantages such as a clear interpretation of the thermophysical model, simple implementation of the separated/homogenous two-phase flow condition, and the same form of all governing equations for both the adiabatic and non-adiabatic capillary flow.

$$\text{Continuity equation: } \frac{\partial \rho}{\partial t} + \frac{\partial (\rho v)}{\partial z} = 0$$

$$\text{Energy equation: } \frac{\partial (\rho E)}{\partial t} + \frac{\partial (\rho v E)}{\partial z} + \frac{\partial}{\partial z}(pv - \tau_{zz} v + q) = \rho v K_z$$

$$\text{Momentum equation: } \frac{\partial (\rho v)}{\partial t} + \frac{\partial (\rho v v)}{\partial z} = -\frac{\partial p}{\partial z} + \frac{\partial \tau_{zz}}{\partial z} + \rho K_z$$

$$\text{Entropy equation: } \frac{\partial (\rho s)}{\partial t} + \frac{\partial (\rho v s)}{\partial z} \geq -\frac{1}{T}\frac{\partial q}{\partial z}$$

The input parameters of the capillary flow simulation are as follows:

- Refrigerant mass flow rate or capillary-tube length;
- Temperature and pressure of subcooled liquid refrigerant at the capillary tube inlet;
- Inner, outer diameter, and wall roughness of the capillary tube;
- Discharge diameter, i.e., approximately the hydraulic diameter of the evaporator;
- Temperature of the capillary inner wall or average ambient temperature around a non-insulated capillary tube;
- Thermophysical properties of the refrigerant considered.

The following simplifications were assumed in our model:

- Capillary flow is solved as one-dimensional steady-state problem;
- Two equilibrium capillary flow regions are considered at the moment;
- Inner, outer diameter, and wall roughness are not varying along the capillary tube length;
- Gravity is not taken into account; the capillary is solved for the horizontal position.

Respecting these simplifications, the governing equations for the *one-phase region* have the following form after the discretization:
Continuity equation (*the same for both capillary flow regions*):

$$\dot{m}_{i+1} - \dot{m}_i = 0 \tag{1}$$

Momentum equation:

$$\left[\dot{m}\, v\right]_{i+1} - \left[\dot{m}\, v\right]_i = -\left[p_{i+1} - p_i\right] A - \tilde{\tau}_{\mathrm{w}} P \Delta z \tag{2}$$

Energy equation for specific energy ($e = h + v^2/2 = E + p/\rho$):

$$\left[\dot{m}\, e\right]_{i+1} - \left[\dot{m}\, e\right]_i = -\tilde{q}_{\mathrm{w}} P \Delta z \tag{3}$$

In a process of discretization of momentum and energy, the adequate formulae are $\partial \tau_{zz} A = -\tilde{\tau}_{\mathrm{w}} P \mathrm{d}z$ and $\partial q A = -\tilde{q}_{\mathrm{w}} P \mathrm{d}z$, respectively.

Enthalpy variations were evaluated by neglecting their dependence on pressure variations: that is $\mathrm{d}h \cong c_p \mathrm{d}T$. The discretized energy equation solved for the control volume outlet temperature gives:

$$T_{i+1} = \frac{\overline{\dot{q}}_{\mathrm{w}} P \Delta z + T_i \overline{\dot{m}} c_p - \overline{\dot{m}} \left( \frac{v_{i+1}^2 - v_i^2}{2} \right)}{\overline{\dot{m}} c_p}. \tag{4}$$

In Eq. 4, $\overline{\dot{q}}_w$ represents the average heat flux over a control volume through the capillary tube wall. The discretized momentum equation solved for the control volume outlet pressure may be expressed as:

$$p_{i+1} = p_i - \frac{\Delta z}{A} \left[ \frac{\dot{m}_{i+1} v_{i+1} - \dot{m}_i v_i}{\Delta z} + \frac{\overline{f}}{4} \frac{\overline{\dot{m}^2}}{2\rho A^2} P \right]. \tag{5}$$

The shear stress at the wall $\tilde{\tau}_{\mathrm{w}}$ in Eq. 2 is given as:

$$\tilde{\tau}_{\mathrm{w}} = \frac{\overline{f}}{4} \frac{\overline{\dot{m}^2}}{2\rho A^2}. \tag{6}$$

Discretized governing equations of the *two-phase region* have the following forms:
Momentum equation:

$$\left[ \dot{m}^{\mathrm{l}} v^{\mathrm{l}} \right]_{i+1} - \left[ \dot{m}^{\mathrm{l}} v^{\mathrm{l}} \right]_i + \left[ \dot{m}^{\mathrm{g}} v^{\mathrm{g}} \right]_{i+1} - \left[ \dot{m}^{\mathrm{g}} v^{\mathrm{g}} \right]_i = -\left[ p_{i+1} - p_i \right] A - \tilde{\tau}_{\mathrm{w}} P \Delta z \tag{7}$$

Energy equation:

$$\overline{\dot{m}} \left( e_{i+1}^{\mathrm{l}} - e_i^{\mathrm{l}} \right) \dot{m}^{\mathrm{g}}{}_{i+1} \left( e_{i+1}^{\mathrm{g}} - e_{i+1}^{\mathrm{l}} \right) - \dot{m}^{\mathrm{g}}{}_i \left( e_i^{\mathrm{g}} - e_i^{\mathrm{l}} \right) = -\tilde{q}_{\mathrm{w}} P \Delta z \tag{8}$$

Entropy creation:

$$\overline{\dot{m}} \left( s_{i+1}^{\mathrm{l}} - s_i^{\mathrm{l}} \right) + \dot{m}_{i+1}^{\mathrm{g}} \left( s_{i+1}^{\mathrm{g}} - s_{i+1}^{\mathrm{l}} \right) - \dot{m}_i^{\mathrm{g}} \left( s_i^{\mathrm{g}} - s_i^{\mathrm{l}} \right) - \frac{1}{T_{\mathrm{w}}} \tilde{q}_{\mathrm{w}} P \Delta z \geq 0 \tag{9}$$

The control volume outlet vapor quality is expressed using the two-phase region discretized energy Eq. 8,

$$x_{i+1}\dot{m}_{i+1}\left[h^{\mathrm{g}}_{i+1}-h^{\mathrm{g}}_{i}+\frac{v^{\mathrm{g}2}_{i+1}-v^{\mathrm{l}2}_{i+1}}{2}\right]=x_i\dot{m}_i\left[h^{\mathrm{g}}_{i}-h^{\mathrm{l}}_{i}+\frac{v^{\mathrm{g}2}_{i}-v^{\mathrm{l}2}_{i}}{2}\right]-\\ -\overline{\dot{m}}\left[c^{\mathrm{l}}_{p}\left(T_{i+1}-T_i\right)+\frac{v^{\mathrm{l}2}_{i+1}-v^{\mathrm{l}2}_{i}}{2}\right]\\ +\overline{\dot{q}}_{\mathrm{w}}P\,\Delta z. \tag{10}$$

The discretized momentum equation, solved for control volume outlet pressure, gives

$$p_{i+1}=p_i-\frac{\Delta z}{A}\left[\frac{\overline{f}}{4}\frac{\overline{\dot{m}}^2}{2\rho A^2}P+\frac{\dot{m}_{i+1}\left\{x_{i+1}v^{\mathrm{g}}_{i+1}+(1-x_{i+1})\,v^{\mathrm{l}}_{i+1}\right\}-\dot{m}_i\left\{x_i v^{g}_{i}+(1-x_i)\,v^{\mathrm{l}}_{i}\right\}}{\Delta z}\right]. \tag{11}$$

The control volume outlet temperature is evaluated from the saturation condition $T_{i+1}=T_{\mathrm{sat}}\,(p_{i+1})$. Discretized Eqs. 4 and 5 for the *one-phase region* and Eqs. 10 and 11 for the *two-phase region* are solved iteratively at each control volume until the demanded convergence criterion is fulfilled. Then the calculation moves further along the capillary tube and the output values at control volume $i$ are taken as initial inputs for volume $i+1$.

The simulation is normally used to solve either the critical length or the critical mass flow rate. These critical conditions are reached just at the control volume, where the entropy creation defined by Eq. 9 is not fulfilled. In this case the capillary flow reaches its critical conditions, and the flow velocity at the capillary outlet is equal to the local speed of sound. At the last step of the calculation, the discharge pressure $p_{\mathrm{dis}}$ at the capillary outlet is compared with calculated outlet pressure corresponding to critical flow conditions $p_{\mathrm{crit}}$. If $p_{\mathrm{dis}} > p_{\mathrm{crit}}$, the flow is non-critical and the sub-critical mass flow rate is solved by using another 'interval-halving' optimization method. A simplified flow chart of the whole model algorithm can be seen in Fig. 5.

### 4.2 Simulation of Different Flow Regimes

The described model based on finite volume discretization is quite flexible in boundary condition definition, as all the governing equations have the same form for both the adiabatic and non-adiabatic case. The heat flux $\overline{\dot{q}}_w$ in Eqs. 4 and 10 is evaluated externally at each control volume and by setting it equal to zero, the adiabatic case of the capillary flow can be solved.

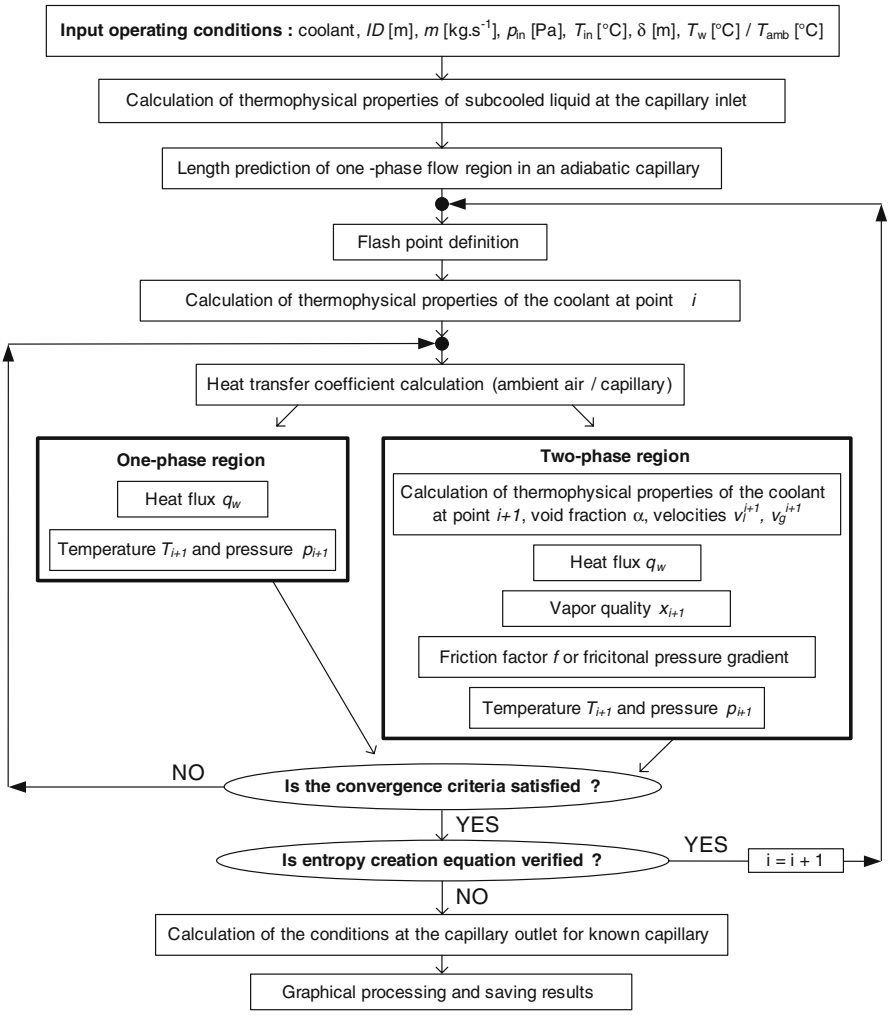


**Fig. 5** Flow chart of the capillary model solved by Matlab program

In a non-adiabatic solution, the heat flux through the capillary wall can be evaluated from two kinds of heat transfer coefficients. The first assumes that the capillary is placed in a heat exchanger; the inner wall temperature is known so that only the forced convection inside the capillary has to be solved. The second corresponds to the case with a non-insulated capillary; natural convection between the ambient and the capillary outer surface, conduction through its wall, and forced convection of flowing refrigerant inside the capillary have to be solved in this case. Simulation of such capillary flow was motivated mainly by the requirement that some of the capillaries are placed as much as 200-m distance from the condenser due to the design of the particle detectors. Hence, the capillary environment has a higher temperature than the temperature of subcooled liquid refrigerant at the capillary tube inlet. The model helped

**Table 1** Summary of the combined parameters for two-phase flow

| Experiment<br>$P_{sat}$=$P_{sat}$ $(T)$ | Experimental data<br>Saturation pressure calculated from the measured temperature | |
|---|---|---|
| Notation | Two-phase multiplier $\Phi_{LO}$ | Slip ratio $S$ |
| *Results of our numerical model* | | |
| Num. model: Lin; Premoli | Lin | Premoli |
| Num. model: Lin; Chisholm | Lin | Chisholm |
| Num. model: Lin; Zivi | Lin | Zivi |
| Num. model: Friedel; Premoli | Friedel | Premoli |
| Num. model: Friedel; Chisholm | Friedel | Chisholm |
| Num. model: Friedel; Zivi | Friedel | Zivi |
| Num. model: Homogeneous | Homogeneous model[a] | $S = 1$ |

[a] In case of homogeneous model $\Phi_{LO}$ is not calculated, friction factor is evaluated from $Re_{TP}$

us to prove that the possible effect of the heat flux between ambient and the non-insulated capillary tube should not greatly affect the mass flow rate delivered through the capillary tube. However, further experimental investigations are under preparation.

The model was tailored to provide capillary flow performance data for the saturated fluorocarbon refrigerants, $C_3F_8$ and $C_4F_{10}$. Theoretical results of our numerical simulation were verified with our own experimental data.

The presented model is structured in such a manner that it is open to further modifications and improvements compared to most other numerical models noted in a literature review. In a further step, two metastable regions of the capillary flow (see Fig. 1b) will be implemented in the model.

## 5 Verification of the Model

Our approach via simulation allows solution of both homogeneous and separated flow through adiabatic or non-adiabatic capillary tubes. Various optional correlations of empirical coefficients were implemented into the model algorithm:

- *Two-phase viscosity*: Mc Adams, Lin, Owen, *Dukler* [15]
- *Friction factor*: Haaland, Churchill, *Colebrook*;
- *Slip ratio*: Chisholm, Zivi, *Premoli* [12];
- *Frictional pressure gradient* (*two-phase multiplier*): Friedel [12], *Lin* [11].

The effects of relevant parameters on the predictions of the capillary flow model were investigated. The correlations by Dukler, Celebrook, Premoli and Lin were chosen as default settings of our model.

The initial evaluation of the presented model was performed for typical refrigerants (R12, R22, and R134a) and compared to available experimental data from the literature. Table 1 summarizes the various parameters in the process of validation.

Some results typical for the refrigerant R12 are shown in Figs. 6 and 7. One can see that the numerical model with a simplified homogeneous two-phase flow region ($v^g = v^l$) reproduces the experimental data reasonably well. Results obtained from the model with separated two-phase flow show some variations. The discrepancies are

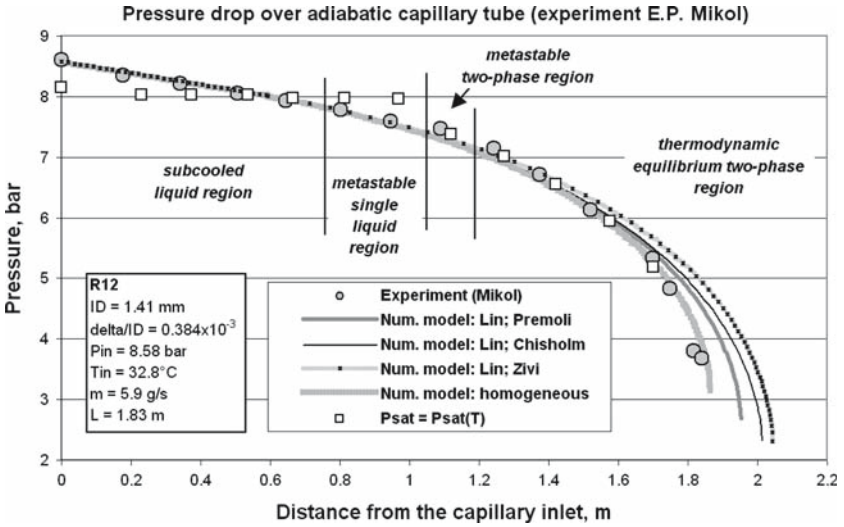


**Fig. 6** Verification of the model and comparison with the experimental data of Mikol [1]

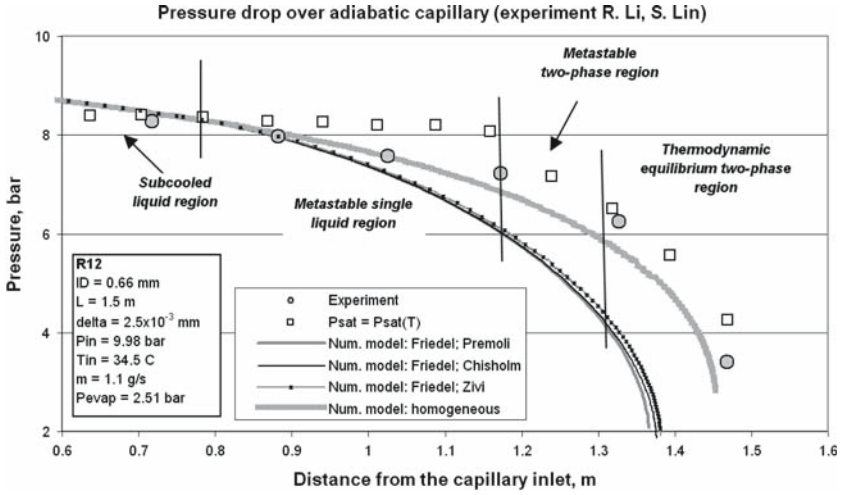


**Fig. 7** Verification of the model and comparison with Li et al. [2] experimental data

caused by the choice of the different approximation of the two-phase multiplier and slip ratio—see Table 1. It can be concluded that the Friedel correlation of the two-phase multiplier [12] usually delivers a higher pressure drop and that consequently the predicted length of the capillary is shorter. Concerning the optimal choice of the parameters for the separated two-phase flow, we would recommend the combination of the Lin two-phase multiplier and the Premoli slip ratio.

## 6 Experimental Verification of the Model

Experimental measurements with two in-house fabricated copper capillaries were performed inside a real circuit operating with $C_3F_8$ and providing us unique conditions of completely dry (oil free) mode. Figure 8 shows a schematic of the circuit.

The circuit with two-stage compression is versatile, allowing changes of parameters such as the inlet pressure (via pressure regulator), evaporation pressure (via back-pressure regulator), and the degree of sub-cooling (realized through a liquid–vapor heat exchanger). Mass flow is recorded via a coriolis mass flow meter in the liquid phase, and could also be checked in the vapor state. The pump allows a rapid increase in the supply pressure if necessary.

The capillary implemented into the circuit for our measurements was divided into uneven length sections where the temperatures were measured with calibrated mini Pt1000 and NTC sensors contacting the inner surface of the capillary. Pressure taps were made with small diameter drills just opposite to the temperature sensor placement. Pressure drops are monitored across the section, and three extra absolute pressure sensors were also installed for reference. The lengths of the section were made larger in the expected liquid-phase flow length and shorter in the expected two-phase flow length as shown in Fig. 9. The uncertainties of all main flow characteristics were predicted to be as follows: pressure $\pm 0.03$ bar, temperature $\pm 0.4$°C, mass flow rate $\pm 0.03\,\mathrm{g \cdot s^{-1}}$. The entire setup was insulated with Armaflex material. The verified ID of the capillary was 1.03 mm, and two lengths ($L_1 \sim 3.25$ m and $L_2 \sim 5.08$ m) were measured in the pilot experimental project. Both capillaries were tested on a liquid phase flow setup before the measurement within the cooling circuit. The relative wall roughness ($\delta / I\,D$), needed for Colebrook's correlation of the friction factor, was found to be 0.0019.

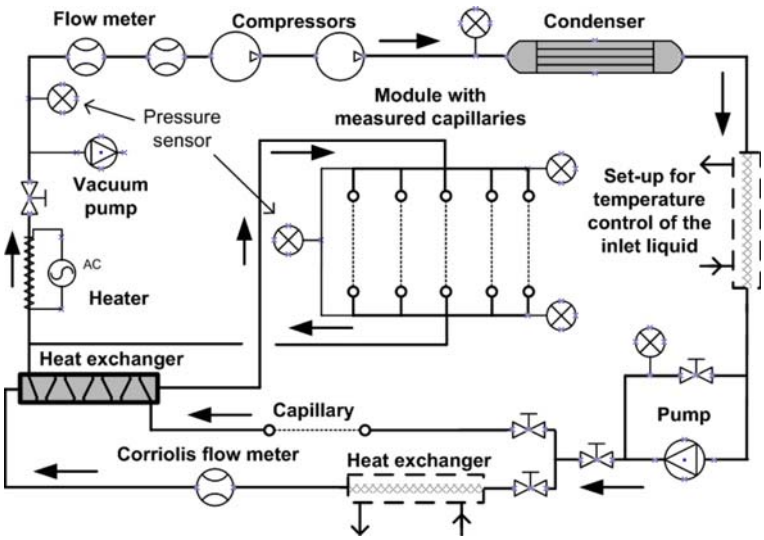


**Fig. 8** Real cooling circuit using the fluoroinert refrigerant $C_3F_8$

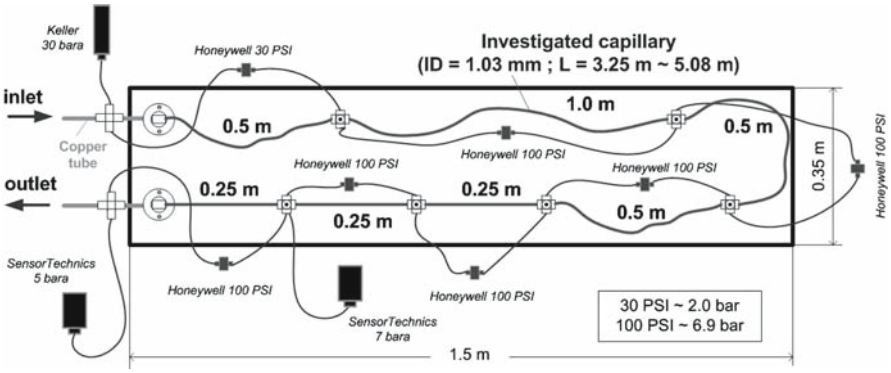


**Fig. 9** Schematics of the model capillary ($ID \sim$ 1.03 mm and $L_1 \sim 3.25$ m, $L_2 \sim 5.08$ m)

The experimentally obtained pressure profile over the capillary installed in the circuit working with $C_3F_8$ refrigerant was compared to the pressure profile predicted by the numerical model. Results with run parameters for the experiment are shown in Fig. 10 for the capillary having a length of 3.25 m and in Fig. 11 for the capillary with a length of 5.08 m.

Reasonably good agreement was found between the experimental results and numerical predictions of the pressure profile, plotted as the solid line. Points corresponding to the saturation pressure were calculated according to the monitored temperature along the capillary. Nevertheless, there are small discrepancies in the expected starting point of vaporization at the end of the liquid flow region between the experimental data and data obtained from the simulation model. More dense sensor placement in the transition region could probably help to clarify it.

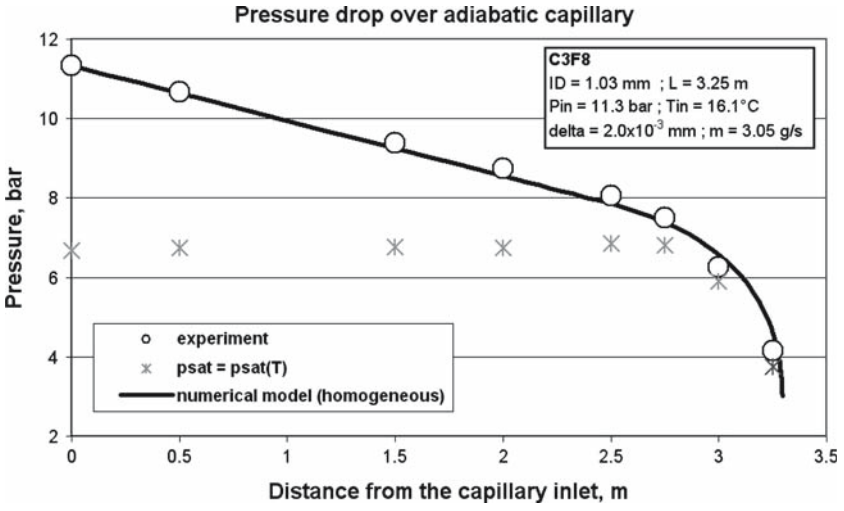


**Fig. 10** Capillary behavior within the circuit/comparison between experimental and predicted data

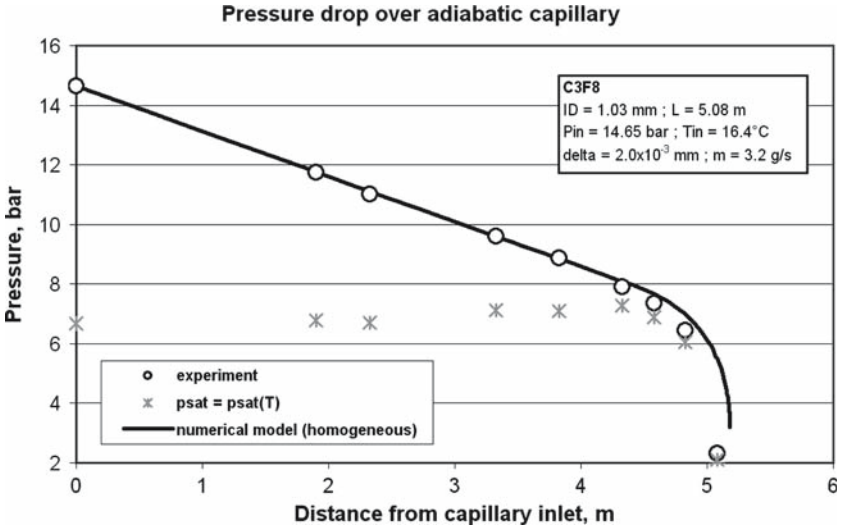


**Fig. 11** Capillary behavior within the circuit/comparison between experimental and predicted data

The numerical model was used to study the influence of the three important parameters for capillary behavior:

(a) *Mass flow of refrigerant*
The increased mass flow decreases both the single-phase and two-phase lengths of the capillary and increases the critical pressure at the capillary outlet. This is illustrated in Fig. 12.

(b) *Inner diameter of the capillary*
It is this primary design parameter of the capillary that influences the capillary flow pattern most significantly. Its combination with capillary length (both for the liquid-phase and two-phase flow) is demonstrated in Fig. 13. There is also an indication that the critical pressure is lower for a larger *ID* where a capillary can eventually become "choked." Curves are plotted for four different *ID*s representing the points at which the model predicts a critical flow condition when the velocity at the capillary outlet reaches the local speed of sound.

(c) *Refrigerant inlet capillary temperature*
With higher sub-cooling of the refrigerant, a lower inlet temperature is achieved and consequently the saturation pressure that indicates the transition region between the one- and two-phase flows is lowered. The ratio between the adequate capillary flow regions changes and the overall usable capillary length increases.

## 7 Conclusion

A numerical model was developed for analyzing the behavior of capillary tubes as throttling devices in cooling circuits operating with saturated fluorocarbon refrigerants. The reliability of the model was verified both with available data from the

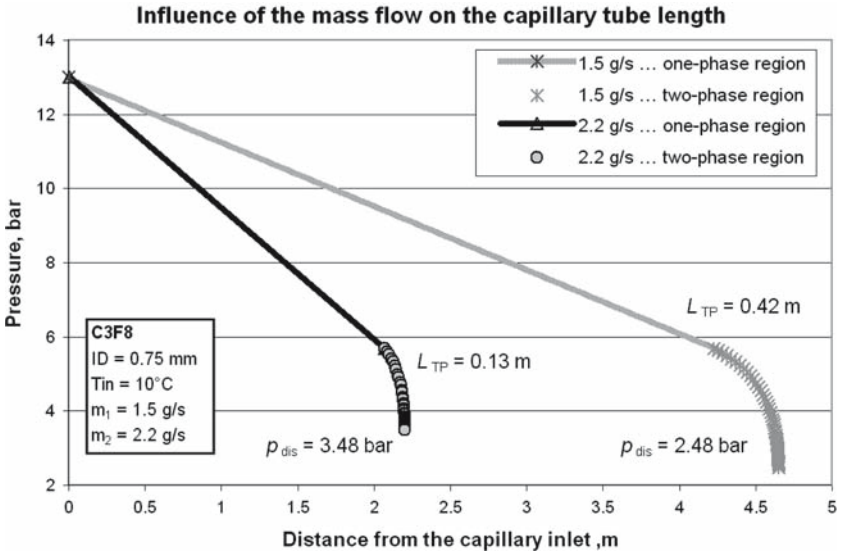


**Fig. 12** Influence of the changed parameters for the capillary flow

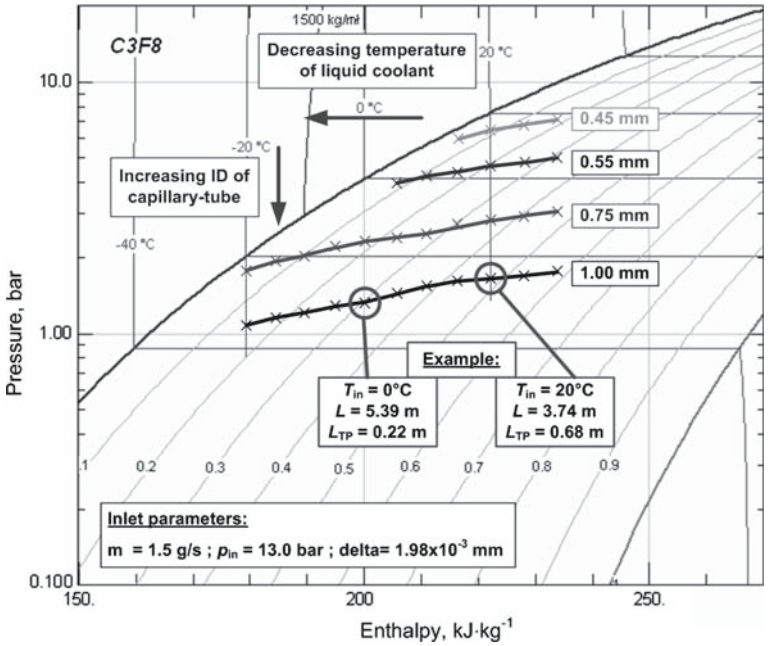


**Fig. 13** Influence of the changed parameters for the capillary flow

literature, for the traditional refrigerants, and comparisons were also performed using our own experimental data obtained from measurements in a real cooling circuit using $C_3F_8$.

The verification or estimation of inner surface capillary roughness and friction factor led us to a detailed investigation of the liquid phase flow through the capillaries via experiment in the single-liquid-flow region.

The generated simulation was successfully used for prediction of the capillary tubes installed in the cooling circuits of 'ATLAS,' 'ALICE,' and 'TOTEM' experiments at CERN laboratory. The model is designed in a versatile form and allows solution of all the main capillary flow cases. It can predict either the mass flow rate through a capillary of given geometry, or the length of a certain capillary that delivers demanded refrigerant at a given mass flow rate. The model provides solutions in both the critical and sub-critical flow regimes. Both the adiabatic and non-adiabatic capillary flow can be solved. Usage of the model significantly reduced the time for trimming of hundreds of the capillaries for use in our applications.

**Acknowledgments** This research was partially supported by the following grants: FRVS Grant—3304006, Grant MSMT CR for the cooperation with CERN—5404003, and VZ-MSMT—J04/98: 212200008. One of the authors, V. Vins is also grateful for support provided by CERN during his stays as a summer student and later as a technical student at that institution.

## References

1. E.P. Mikol, J. ASHRAE 75–86 (1963)
2. R.Y. Li, S. Lin, Z.Y. Chen, Z.H. Chen, Int. J. Refrig. **13**, 181 (1990)
3. Z.H. Chen, R.Y. Li, S. Lin, Z.Y. Chen, ASHRAE Trans. **96**, 550 (1990)
4. C. Lackme, Int. J. Multiphase Flow **5**, 131 (1979)
5. H. Koizumi, K. Yokoyama, ASHRAE Trans. **86**, 19 (1980)
6. P.K. Bansal, A.S. Rupasinghe, Appl. Therm. Eng. **18**, 207 (1998)
7. P. Kritsadathikarn, T. Songnetichaovalit, N. Lokathada, Res. Article, Sci. Asia **28**, 71 (2002)
8. S.M. Sami, C. Tribes, Appl. Therm. Eng. **18**, 491 (1998)
9. T.N. Wong, K.T. Ooi, Appl. Therm. Eng. **16**, 625 (1996)
10. Z.L. Miropolskiy, R.I. Shneyerova, A.I. Karamysheva, in *International Heat Transfer Conference*, vol. 5 (Paris, 1970), Paper B 4.7
11. S. Lin, C.C.K. Kwok, R.Y. Li, Z.H. Chen, Z.Y. Chen, Int. J. Multiphase Flow **17,** 95 (1991)
12. S. Wongwises, P. Chan, Int. Comm. Heat Transfer **27**, 343 (2000)
13. P.K. Bansal, G. Wang, Appl. Therm. Eng. **24**, 851 (2004)
14. J. Sinpiboon, S. Wongwises, Appl. Therm. Eng. **22**, 2015 (2002)
15. F. Escanes, C.D. Pérez-Segarra, A. Oliva, Int. J. Refrig. **18**, 113 (1995)
16. V. Gnielinski, Int. Chem. Eng. **16**, 359 (1976)
17. O. García-Valladares, C.D. Pérez-Segarra, A. Oliva, Appl. Therm. Eng. **22**, 173 (2002)
18. B. Xu, P.K. Bansal, Appl. Therm. Eng. **22**, 1801 (2002)
19. T. Yilmaz, S. Ünal, ASME J. Fluids Eng. **118**, 150 (1996)
20. C. Zhang, G. Ding, Int. J. Refrig. **27**, 17 (2004)
21. C. Melo, R.T.S. Ferreira, C. Boabaid Neto, J.M. Concalves, Appl. Therm. Eng. **19**, 669 (1999)
22. M.O. McLinden, S.A. Klein, E.W. Lemmon, A.P. Peskin, *REFPROP Version 6.0* (National Institute of Standards and Technology, Gaithersburg, Maryland, 2000)
23. V. Vacek, G. Hallewell, S. Lindsay, Fluid Phase Equilib. **185**, 305 (2001)
24. V. Vacek, G. Hallewell, S. Ilie, S. Lindsay, Fluid Phase Equilib. **174**, 191 (2000)
25. S.D. Chang, S.T. Ro, in *1996 International Refrigeration Conference*, vol. 83 (Purdue Univ., Lafayette, Indiana, 1996)